JOURNAL OF MATERIALS SCIENCE **34** (1999) 4633–4638

Corrosion resistance and microstructure of stainless steel modified by pulsed high energy density plasma

WEI KUN, WU XINGFANG, FU YING
Department of Materials Physics, University of Science and Technology, Beijing, 100083 Beijing, People's Republic of China

YANG SI-ZE, LI BING
Institute of Physics, Chinese Science Academy, 100080 Beijing, People's Republic of China

Pulsed high energy density plasma has been used to deposit aluminum nitride films on the surface of the 1Cr18Ni9Ti stainless steel (∼0.1% C, ∼18% Cr, ∼9% Ni, ∼0.8% Ti). The formed films are composed of nanocrystalline-structured aluminum nitride phase, whose crystal sizes are about 10 nm. Transition areas are formed across the film to the substrate and strengthen the adhesion between them. The nanocrystalline-structured aluminum nitride films contribute to the improvement of the corrosion resistance of the modified stainless steel, whose corrosion rate has been reduced by about ten times compared with that of the unmodified stainless steel.

1. Introduction

Improving the corrosion resistance ability of steel surface is an important way to extend steel application. Various methods, for example, nitriding treatment of steel surfaces [1] and deposition of metal nitride films (including titanium nitride (TiN), aluminum nitride (AlN) and chromium nitride (CrN)) [2], have been used to improve the corrosion resistance and fatigue resistance of steel surface. Aluminum nitride film is a kind of anticorrosive film, whose high thermal and chemical stability explain its wide use in functional coating and device [3]. It has high corrosion resistance against molten aluminum alloys and oxidation up to 700 °C [4]. It has been deposited by CVD [5], r.f. sputtering [6, 7] and reactive molecular beam epitaxy surface modification methods [8]. However, in some of the mentioned methods, the heating of substrate to high temperature to strengthen the adhesion of film to substrate might affect the properties of the substrate material. While in the pulsed high energy density plasma (PHEDP) surface modification method, this problem has been avoided.

Pulsed high energy density plasma has been used to form films, such as titanium carbonitride (TiCN) film [9] and cubic boron nitride (C-BN) film [10]. In PHEDP surface modification, it is not necessary to heat the substrate to strengthen the adhesion between the film and the substrate because the plasma can heat the surface of the substrate to 1500 °C very quickly and change it into molten state without influencing the general characteristics of the whole body of the substrate. The molten surface cools down rapidly if the substrate material has good thermal conductivity (such as steel) and the cooling rate can reach 1.01×10^8 °C/s [9], which is much more quicker than what is need in steel quenching. In addition, the ion implantation effect by active plasma particles, whose elemental compositions can be selected according to needs, accompanies the quenching process of PHEDP.

In this paper, the pulsed high energy density plasma composed of particles of aluminum and nitrogen has been used to form aluminum nitride films on 1Cr18Ni9Ti(∼0.1% C, ∼18% Cr, ∼9% Ni, ∼0.8% Ti) stainless steel. The anticorrosion ability and the microstructure of the modified steel have been studied.

2. Experimental details

The process of PHEDP surface modification is schematically shown in Fig. 1 [9]. The operating gas is introduced through an electromagnetic valve, and the adjustable operating voltage is maintained across the outer and inner aluminum electrodes. Once the gas flows into the coaxial gun, it breaks down and large electric current flows through the end of the coaxial gun, which helps the generation of the metal particles by sputtering and evaporation. The plasma, created by the discharge and composed of particles of aluminum and nitrogen, is heated by the Joule heating and accelerated by the Lorentz force $J \times B$ to the sample.

Specimens of 1Cr18Ni9Ti stainless steel were cut into disks of ($\Phi 30 \times 7$) mm, then the disks were impacted by PHEDP. The parameters of PHEDP treatment are listed in Table I. Sample 1 is unmodified stainless steel. Sample 2 is PHEDP modified stainless steel. Each of the samples (sample 1 and sample 2) is divided into four parts: two of them are used for corrosion test, and the remains are used for the preparation of the transmission electron microscope (TEM) specimens.

TABLE I Parameters of the PHEDP processing

Samples		Plasma parameters		
No.	State	Discharge voltage (kV)	Nitrogen pressure (kg/m^2)	Pulse number
Sample 1	Unmodified stainless steel	—	—	—
Sample 2	PHEDP modified stainless steel	1.5	1.0	50

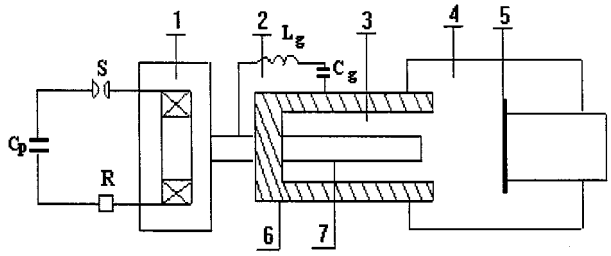

Figure 1 Schematic diagram of generating pusled plasma and surface processing: (1) electromagnetic valve, (2) charging and discharging circuit, (3) coaxial plasma gun, (4) vacuum chamber, (5) sample, (6) outer electrode, (7) inner electrode.

The specimens to be used in corrosion test are prepared as follows: for each part of unmodified stainless steel (sample 1), arbitrarily leave one face for corrosion test and coat the other faces with epoxy; for each part of the PHEDP modified stainless steel (sample 2), leave the film face for corrosion test and coat the other faces with epoxy. In our experiment the faces left for corrosion test have equal area. The prepared samples undergo electrochemical corrosion test [11]. The corrosion solution is 2% NaCl solution. The tests were performed on M351 potentiostat instrument that is used in conjunction with a computer and an X-Y recorder to plot Tafel curves. Tafel curves are got by testing the corrosion current density versus the corrosion potential in the rang of $\pm$100 mV around the free corrosion potential and are used to exhibit the corrosion resistance of the samples by showing their free corrosion potentials (E_{corr}) and corrosion rates. The free corrosion potentials are checked out at the beginning of corrosion test and shown by Tafel curves (shown as following), the corrosion rates are denoted by the free corrosion current

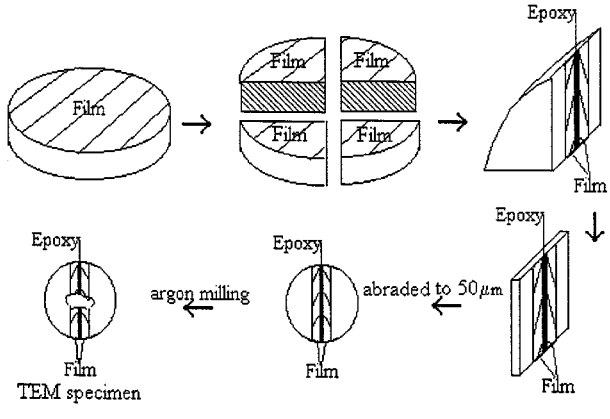

Figure 2 The schematically show of the process of specimen preparation for TEM observation.

TABLE II Results of the corrosion resistance test

Samples	Free corrosion potential E_{corr} (mV)	Free corrosion current density i_{corr} (A/cm^2)	Surface appearance after corrosion test
Sample 1	$-$ 199.0	3.98×10^{-7}	No corrosion spots
Sample 2	$-$ 156.0	3.16×10^{-8}	No corrosion spots

densities (i_{corr}) that are calculated from the expolation Tafel curves by computer.

TEM specimens are prepared according to cross-section method (as shown in Fig. 2). The film sides are glued together, then the glued body is cut into slips of 0.2 mm thickness by electric spark working, and the slips are mechanically abraded to 50 μm thickness and then milled by argon milling. The TEM observation is performed on JEOL100CX and JEOL2000FX.

3. Results

The results of corrosion section test are shown in Fig. 3 and Table II. Fig. 3 shows the Tafel curves of sample 1 (curve *a*) and sample 2 (curve *b*), and Table II shows the values of E_{corr} and i_{corr} and the surface appearance of the samples. It can be seen in Table II that the free corrosion current density (i_{corr}) of sample 2 has been reduced by about ten times compared with that of sample 1, and the E_{corr} value of sample 2 is more positive than that of sample 1. The value of i_{corr} stands for corrosion rate, and small value of i_{corr} implies low corrosion rate. The value of E_{corr}, stands for resistance ability against the start of corrosion. The phase with more positive E_{corr} value has relatively higher resistance ability because of its high Gibbs free energy [11]. Therefore the corrosion rate of sample 2 have been reduced by about one order compared with that of sample 1, and the resistance ability to the corrosion start of sample 2 is higher than that of sample 1. Thus, the PHEDP surface modification improved the corrosion resistance of surfaces of 1Cr18Ni9Ti stainless steel.

The results of TEM observation of the PHEDP modified steel (sample 2) are shown in Figs 4 to 7. Fig. 4a is selected area diffraction pattern (SAD) of cubic aluminum nitride phase in the film, and Fig. 4b is the central dark field image (CDF) of aluminum nitride. Fig. 5 shows the results of the TEM observation of the structural transformation from the film to substrate. Fig. 5d is the schematically show of the TEM specimen. A, B and C are the sites along the thin areas from film to substrate. Fig. 5a, b and c are the SAD patterns obtained at area A, area B and area C, respectively. Fig. 5a* and b* are the central dark field images taken with the diffraction of AlN phase. The indexing of the rings in Fig. 5 is shown in Table III. Fig. 6a is the SAD pattern of iron nitride phase in the film, whose indexing is shown in Table IV, and Fig. 6b is the CDF of iron nitride phase. It can be seen from Figs 5 and 6 that the structural transformations from the film to the substrate are gradually and transition areas are formed across the film to the substrate as denoted by area C. The transition areas are constitute of aluminum nitride, iron nitride and austenite phases. As illustrated in Figs 4b and 6b, the particle

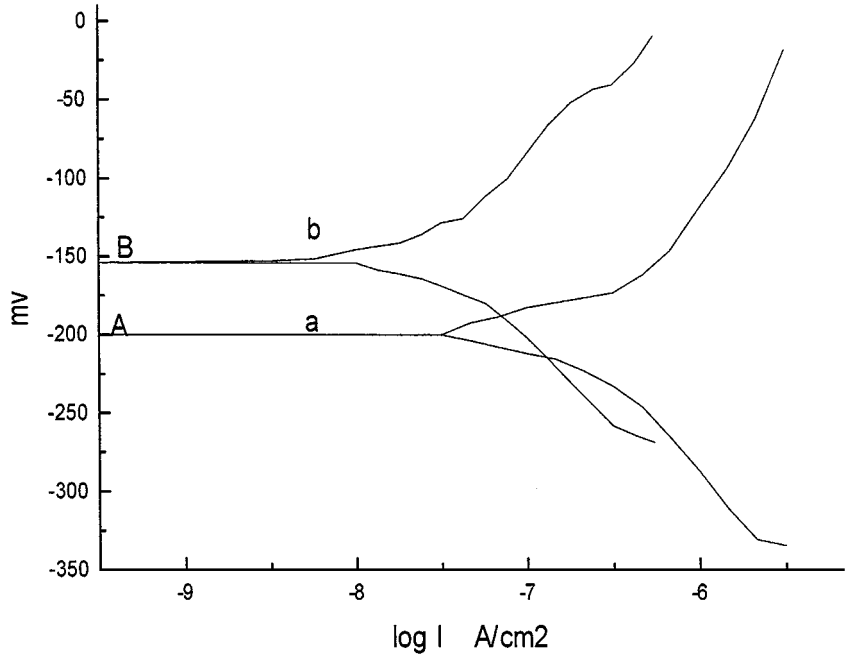

Figure 3 Tafel curves of samples: (a) sample 1 (unmodified steel), (b) sample 2 (PHEDP modified steel), *the ordinate values of point *A* and *B* are the values of the free corrosion potential (E_{corr}) of sample 1 and sample 2 respectively.

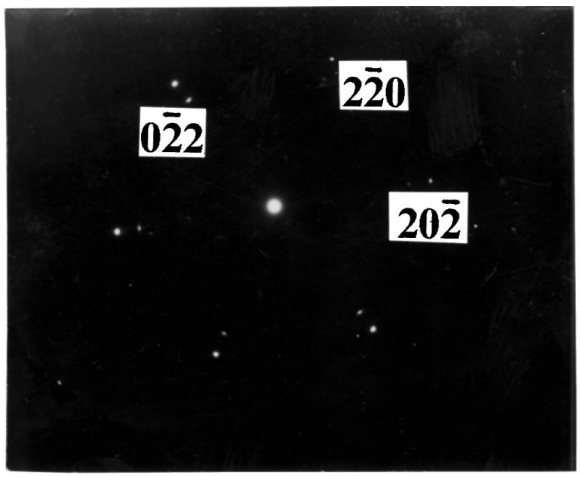

(a)

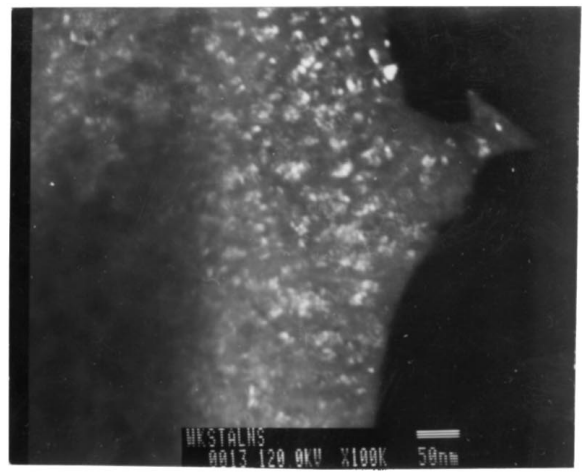

(b)

Figure 4 (a) Selected area diffraction (SAD) pattern of AlN and austenite phase of sample 2, (b) Central dark field image (CDF) of AlN phase taken with the weak point of a 220 type reflection of AlN of sample 2.

TABLE III Indexing of the diffraction pattern in Fig. 5 (Lλ = 2.20 nm.mm)

Ring no.	Ring diameter 2r (mm)	Crystal plane distance, *d* (nm) Experimental value	[a]JCPDS values AlN	[a]*hkl* AlN
1	18.5	0.238	0.2379	111
2	21.0–24.0	0.209–0.187	0.2060	200
3	30.5	0.144	0.1457	220

[a]JCPDS card values are from AlN(25-1459), *hkl* is the index of crystal plane.

sizes of aluminum nitride and iron nitride are about 10 and 50 nm, respectively. Fig. 7 shows the results of the study of the compositional transformation from film to substrate by the energy dispersion spectrum (EDS)

TABLE IV Indexing of the diffraction pattern in Fig. 6 (Lλ = 2.096 nm.mm)

Ring no.	Ring diameter 2r (mm)	Crystal plane distance, *d* (nm) experimental value	[a]JCPDS values γ-Fe	Fe_3N	[a] *hkl* γ-Fe	Fe_3N
1	18.0–20.0	0.233–0.210		0.2380		100
				0.2190		002
			0.2080	0.2090	111	101
2	22.2	0.189	0.1800		200	
3	28.0	0.155		0.1610		102
4	32.0	0.132		0.1370		110
5	34.5	0.122	0.1270	0.1240	220	103
6	37.2	0.113		0.1140		112
7	39.5	0.106	0.1083	0.1040	311	202

[a]JCPDS card values are from γ-Fe(23-298) and Fe_3N (1-1236), *hkl* is the index of crystal plane.

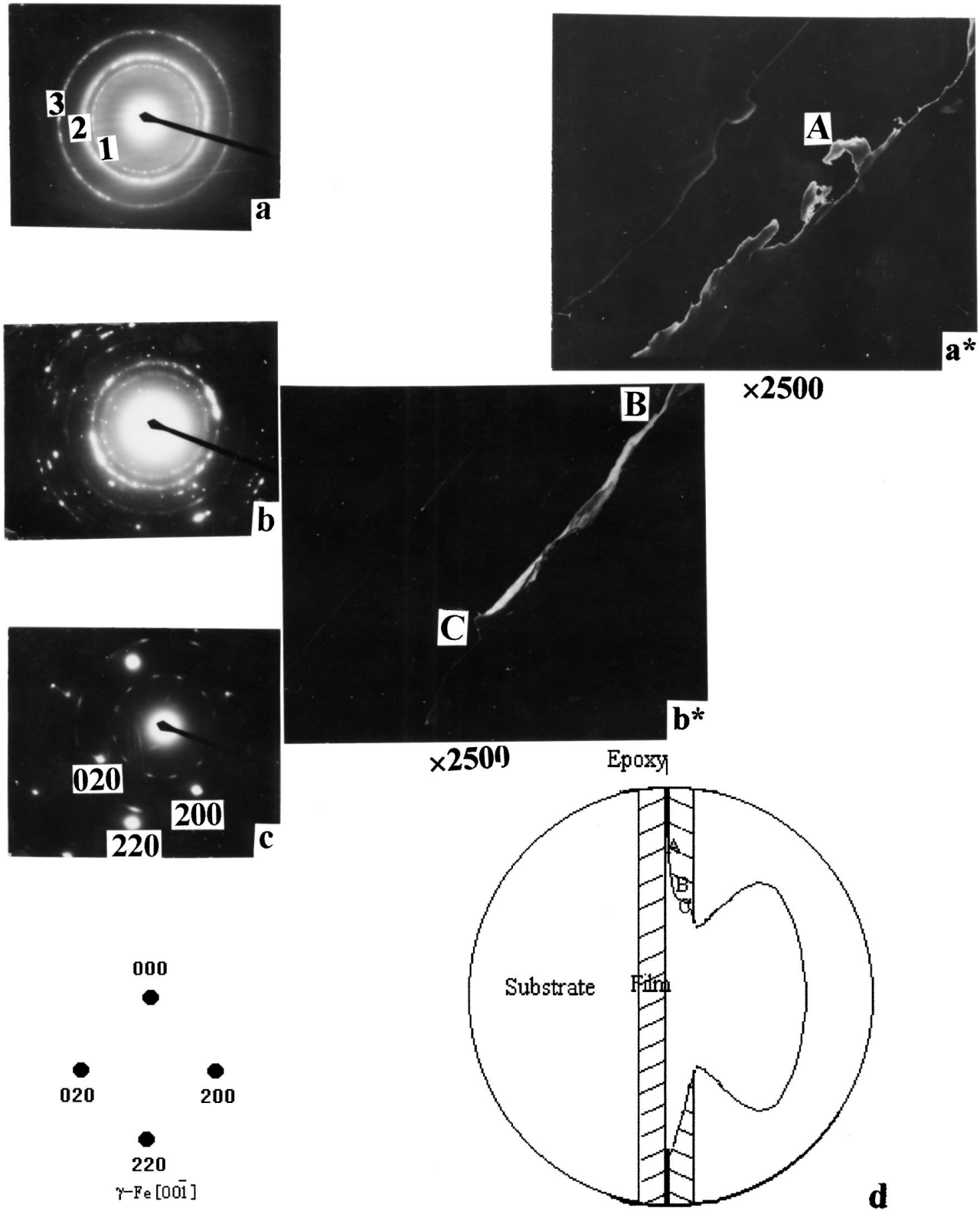

Figure 5 The transition from film to substrate shown by TEM: (a) SAD pattern obtained at area A, (b) SAD pattern obtained at area B, (c) SAD pattern obtained at area C, (d) the schematically show of the TEM specimen. a' and b' are the central dark field image taken by the type 111 reflection of aluminum nitride phase.

analysis via TEM. Table V shows the results of EDS of area A, area B and area C, respectively. It shows that the content of aluminum decreases from area A to area C gradually.

4. Discussion

The electrochemical corrosion of steel is usually produced by the formation of microcorrosion cells caused by the potential difference at the steel surface due to the heterogeneity of the microstructure, composition or stress. The electrochemical corrosion reaction in neutral solution (salt solution, for example) is as following [12]:

$$\text{Anodic reaction} \quad Fe \rightarrow Fe^{2+} + 2e$$

$$\text{Cathodic reaction} \quad \tfrac{1}{2}O_2 + H_2O + 2e \rightarrow OH^-$$

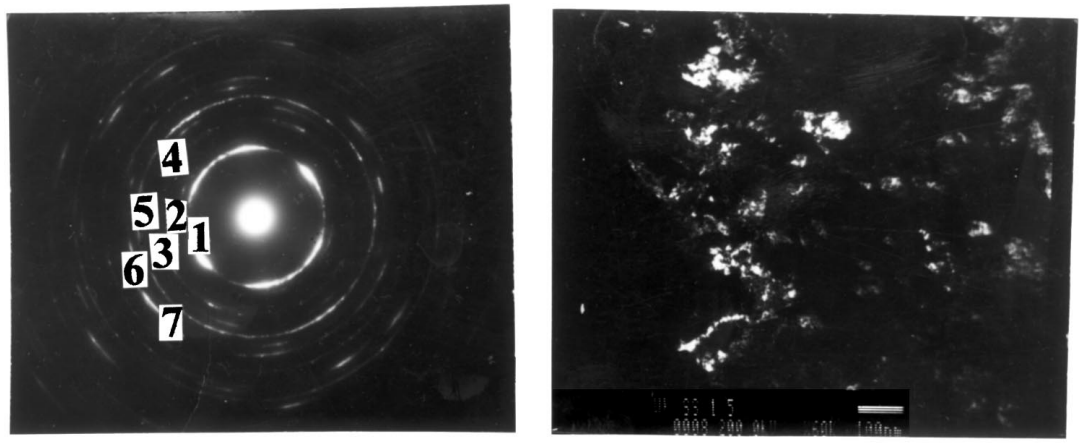

Figure 6 (a) SAD of Fe_3N and austenite in the transition area of sample 2 (b) CDF of Fe_3N taken with a 100 type reflection of Fe_3N of sample 2.

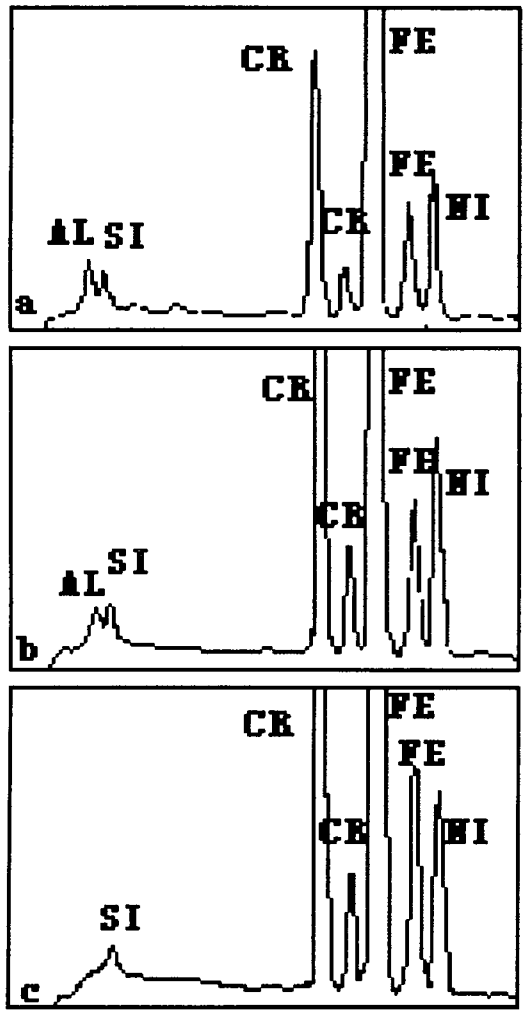

Figure 7 (a) Energy dispersion spectrum (EDS) taken at area A, (b) Energy dispersion spectrum (EDS) taken at area B, (c) Energy dispersion spectrum (EDS) taken at area C.

TABLE V The results of quantitative analysis of EDS of Fig. 7

[a]Element line	At %			Element wt %		
	area A	area B	area C	area A	area B	area C
Fe-K	64.18	65.26	67.77	66.97	67.10	67.77
Cr-K	18.72	19.32	20.19	18.14	18.44	19.18
Ni-K	10.45	11.52	9.37	11.49	12.48	10.10
Al-K	3.90	1.37	0.59	1.96	0.68	0.29
Si-K	2.74	2.53	2.09	1.43	1.30	1.07

[a]Element line stands for the K series of the irradiated X-ray of the elements.

In the anodic reaction iron atoms lose electrons and dissolve into the solution. The depolarization element OH^- transfers electrons to the cathode.

1Cr18Ni9Ti stainless steel, which is composed of austenite phase, is free from the corrosion caused by the formation of microcorrosion cell due to the potential difference between two phases. Therefore it has relatively high corrosion resistance in steel family. But in solutions including Cl^-, such as NaCl solution, because the radium of Cl^- is very small, it penetrates in, and leads to the corrosion of the stainless steel. To improve corrosion resistance of the stainless steel, PHEDP surface modification method is used to form aluminum nitride film on the steel surface.

Aluminum nitride film has good mechanical, optical properties and good corrosion resistance in molting metal fluid [3, 4]. It has high Gibbs free energy [13], which makes it stable in chemical reactions. In addition, TEM studies showed that the formed film by PHEDP is composed of nanometer-sized aluminum nitride phases. The formation of the nanocrystalline structure of AlN is due to the high cooling rates (produced by PHEDP on steel surface) making the nucleation rate of AlN high enough to form nanocrystals. It has been proved that nanocyrstalline materials (whose crystal sizes are around 10 nm) have superior localized corrosion resistance compared to the conventional polycrystalline materials, even though the composition of both is the same [14, 15]. The nanocrystalline materials have relatively much more intergranular area compared with conventional polycrystalline materials. According to theory, it has been shown that the intercrystalline (grain boundary and triple junction) content of a material increases from a value of 0.3% at a grain size of 1 μm to more than 50% at grain sizes less than 5 nm [16]. Therefore, the nanocrystalline material has evenly distributed defect sites (e.g. grain boundary), and thus it corrodes uniformly on all exposed surface.

Furthermore, the grain boundaries of nanocrystals are low in energy, thus, they are not so active as that of conventional polycrystalline structures [17, 18]. Consequently, the formed nanocrystalline-structured aluminum nitride films contribute to the improvement of the corrosion resistance of the stainless steel.

The formed film adhered strongly to the substrate because transition areas were formed between the film and the substrate, whose microstructures are the combination of the aluminum nitride, iron nitride and austenite. Moreover, the particle sizes of the aluminum nitride phase at the film surface are smaller than those in transition area because the amount of the nuclei of aluminum nitride phase in transition area is less than that of film surface, which is displayed by the change of the diffraction pattern of aluminum nitride phase from smoothing rings to dash rings as shown in Fig. 5. The formation of iron nitrides is because the iron ions that have been sputtered out from the substrate reacted with the nitrogen ions that implant in. The results of TEM observation and EDS analysis show that, on steel surface, the PHEDP modification formed an adhesive AlN film whose structure and composition change to the substrate by degrees.

5. Conclusion

From the results above, the following conclusions can be established:

(1) 1Cr18Ni9Ti stainless steel modified by PHEDP has improved corrosion resistance ability in 2% NaCl solution. Its corrosion rate has been reduced by about one order compared with that of unmodified 1Cr18Ni9Ti stainless steel.

(2) TEM studies show that the formed film is composed of nanometer-sized aluminum nitride phases. The high cooling rate produced by PHEDP on the steel surface contributes to the formation of the nanocrystalline structures. The films have strong adhesion to substrate due to the formation of transition areas across the film to substrate. The transition areas are constituted of aluminum nitride, iron nitride and austenite. The compositional and structural transformations from film to substrate are gradually.

(3) The improvement of the anticorrosion ability of 1Cr18Ni9Ti steel is due to the formation of the adhesive aluminum nitride films that are stable in the chemical reaction. Its nanocrystalline structure has improved resistance to the localized corrosion compared with the conventional crystalline structure.

Acknowledgement

The authors would like to acknowledge to the financial support provided by the National Nature Science Foundation of China and the International Atomic Energy Agency.

References

1. H. V. BOENING, "Plasma Science and Technology" (Cornell University Press, Ithaca and London, 1982) p. 266.
2. D. M. MOTTOX, J. E. GREENE, D. H. BUCLEY and G. A. SOMORJAI, *Mater. Sci. & Eng.* **70** (1985) 79–89.
3. H. TAKAOKA, *Thin Solid Films* **157** (1988).
4. Y. G. ROMAN and A. P. M. ADRIAANSEN, *ibid.* **169** (1989) 241–248.
5. J.-G. KIM, C.-S. DARK and J. S. CHUN, *ibid.* **97** (1982) 97.
6. R. MACMAHON, J. AFFIMITO and R. PARSONS, *J. Vac. Sci. Technol.* **20** (1982) 376.
7. G. ESTE, R. SURRIGE and W. D. WESTWOOD, *ibid.* **A3**(4) (1986) 989.
8. F. ALEXANDRE, J. M. MASSON and A. SCAVENNE, *Thin Solid Films* **1**(98) (1982) 75.
9. P. X. YAN, S. Z. YANG and X. S. CHEN, *Acta Metall. Sinica* **11**(50) (1994) 24–27.
10. P. S. YAN, S. Z. YANG, B. LI and X. S. CHEN, *Phys. Stat. Sol. (a)* **145** (1994) K29.
11. L. L. SHREIR, "Corrosion" (George Newnes Ltd., London, 1983) p. 21.10.
12. L. J. KORB and D. L. OLSON, "Metals Handbook" (Metals Park, Ohio, 1987) p. 511.
13. J. LIANG and Y. CHE, "Wujiwu Relixue Shuju Shouce" (Northeast University Press, Beijing, 1993) p. 51.
14. LU KE and ZHOU FEI, *Acta Metall. Sinica* **33** (1997) 99–106.
15. R. B. INTURI and Z. S. SMIALOWSKA, *Cossion* **5**(48) (1992) 398–403.
16. G. PAULUMBO, S. J. THORPE and K. T. AUST, *Script. Metall. et Material* **24** (1990) 1347–1350.
17. G. J. THOMAS, R. W. SIEGEL and J. A. EASTMAN, *ibid.* **24** (1990) 201.
18. J. WANG, D. WOLF and S. R. PHILLPOT, *Philosophy Magazine A* **73** (1996) 517.

Received 18 November 1998
and accepted 8 April 1999